Sensors and Materials, Vol. 35, No. 8 (2023) 3071–3082
MYU Tokyo

S & M 3375

Predicting Band Structures of Two-dimensional Phononic Crystal Slab for Sensor Predesigning Based on Artificial Neural Network

Chi-Tsung Chiang,[1] Ying-Pin Tsai,[2] Wei-Shan Chang,[1] and Fu-Li Hsiao[1*]

[1]Institute of Photonics, National Changhua University of Education,
No. 1 Jin-de Road, Changhua City, Changhua County, 50007 Taiwan (R.O.C)
[2]Institute of Imaging and Biomedical Photonics, National Yang Ming Chiao Tung University,
Chi-Mei Building, No. 301, Sec. 2, Gaofa 3rd Road, Guiren Dist., Tainan City 71150, Taiwan (R.O.C.)

(Received December 30, 2022; accepted July 12, 2023)

Keywords: phononic crystals, phononic band structures, neural networks

A phononic crystal is an artificial material with spatially elastic modulus usually designed for sensing. By using Bloch's theorem and the concept of the Brillouin zone, the phononic band structure can be obtained. The phononic crystal slab is formed by arranging two-dimensional periodic structures in an elastic slab. The periodic structure can control the propagation direction of the elastic wave, which is parallel to the slab and has great potential for many applications. However, it is time-consuming to determine the proper design. The artificial neural network is a promising tool for solving complex problems. We aim to train a neural network to predict the phononic band structure of silicon phononic crystal slabs. The training data are obtained by the finite element method. Our results show that the proposed artificial neural network can rapidly predict the eigenfrequencies of the band structure with high accuracy.

1. Introduction

Phononic crystals are artificial materials with spatially periodic elastic moduli.[1,2] The special sound wave modulation ability enables good design of phononic crystals for sensing.[3,4] Before using the phononic resonator to design specific sensors, the fundamental characteristics of the phononic crystals should first be investigated. The elastic moduli include mass density and elastic coefficient. The concept of the phononic crystal is inspired by photonic crystals.[5] In the photonic crystal, the spatially periodic refractive index distribution generates "photonic band gaps". Optical waves cannot propagate in the photonic crystal when their frequencies are within the band gap range. Photonic band gaps are similar to the energy gap of electrons in semiconductors. The electrons in semiconductors are regarded as electron waves, which are governed by the Schrödinger equation. The energy gap of electrons in a semiconductor can be derived by setting the potential to be spatially periodic. The mathematical format of the Schrödinger equation is the same as that of the optical wave equation. Therefore, the periodic

*Corresponding author: e-mail: fulihsiao@cc.ncue.edu.tw
https://doi.org/10.18494/SAM4515

ISSN 0914-4935 © MYU K.K.

distribution of the refractive index leads to the photonic band gap. There are many analogies between optical and acoustic waves. The periodic elastic moduli also lead to phononic band gaps. In addition, the acoustic waves have more polarization than the optical waves, and the elastic modulus have more variables than the refractive index used in optics. Therefore, the phononic crystal structures and devices have high diversity.

The periodic elastic moduli in the phononic crystal structure are usually generated by integrating two different materials periodically. The materials used in phononic crystals can be solid/solid, solid/liquid, or solid/air. Because of the variety of material combinations, the phononic crystal can be applied in many fields, such as underwater ultrasonic devices[6] and surface acoustic wave devices.[7] One of the potential applications is micro–mechanical resonators,[8] which are commonly used in communications and micro–electromechanical systems (MEMSs). Recently, the optical-mechanical transducer that can convert the information carried by optical waves into that carried by mechanical waves[9] has been extensively studied. Such an optical-mechanical transducer plays a key role in quantum computing.[8] The phononic-crystal-based micro–mechanical resonator is usually formed by arranging periodic air holes on a mechanical waveguide, such as a membrane, a slab,[10] or a nanobeam.[11] The mechanical waveguide can confine the propagation of acoustic waves to the in-plane direction. The periodic air holes can be used to further manipulate the guided acoustic wave via the phononic band gap effect.[12] The mechanical resonator can be realized by intentionally introducing suitable defects into the periodic structure. These kinds of resonators usually have higher quality factors than traditional micro–mechanical resonator devices. In addition, some novel designs can be achieved by using phononic crystals, such as acoustic metamaterials based on local resonance,[13] the negative refraction effect,[14] and the topological phononic crystal structure.[15] The abovementioned applications, devices, and phenomena are all related to the phononic band structure, whose diagram represents the dispersion relations of acoustic waves propagating in all directions within the phononic crystal. The shapes, slopes, and frequencies of phononic bands define the band gap range, group velocities, and directions of energy flow of acoustic waves. The phononic band structure can be tailored by modifying the geometric configuration and elastic moduli of the phononic crystal. However, the relationships between the phononic band structure and the geometric and elastic parameters are complex and nonlinear, making it difficult to define design rules. The anticipated phononic structures are usually obtained by repeatedly modifying parameters and calculating the corresponding band structures, which is time-consuming.

Deep learning has been attracting extensive attention recently. Deep learning and an artificial neural network (ANN) are powerful tools for solving complex and nonlinear problems such as image processing, optical sensing, and optical device design.[16–19] ANN-based deep learning enables the mapping of the input and output information of complex structures or devices. For example, the ANN is used for determining the state of analyte using the ergodic spectra of sensors. It does not need to extract the features of the spectra. The ANN can also predict the features of the photonic band structures of photonic crystals using geometric and optical parameters. The calculation process is significantly faster than those of traditional methods. Because the design of the phononic crystal structure requires extensive calculation, the ANN

and deep learning are also introduced to assist this process. For example, Li *et al.* used the ANN to generate the possible shapes of the unit cell of a phononic crystal on the basis of the anticipated phononic topological and band gap properties.[20] Han *et al.* used deep learning with the anticipated wave attenuation to design a phononic crystal.[21]

The previous studies of phononic crystals with deep learning usually focused on the relationships between certain acoustic properties and the configurations of structures. However, the prediction of whole band structures is also an important task. Many important features of phononic crystals, such as slow acoustic modes, topological phononic crystal, and negative refraction, are related to full phononic band diagrams. Whole band structure prediction can significantly reduce the design schedule. Our aim is to use the ANN-predicted whole phononic band structure based on the geometric parameters of a two-dimensional silicon phononic crystal slab.

2. Band Structure Calculation and ANN Configurations

In this study, we focus on the phononic crystal band structures of two-dimensional silicon phononic crystal slab structures. The structures are formed by arranging two-dimensional periodic air cylinders in a silicon slab. We use two kinds of periodic structures of the air cylinder array: square and triangular lattices. The unit cells of the square and triangular lattices are shown in Figs. 1(a) and 1(b), respectively. The phononic crystal slab is formed by arraying these unit cells periodically in the *x*-*y* plane. The lattice constants (marked by "a") of the square and triangular lattices are both 500 μm. The thickness of the slab is denoted by "H" and the radius of an air cylinder is denoted by "r". The operating frequency ranges are in the MHz region, which is a common frequency range for MEMS systems and optomechanical coupling applications. According to the Bloch theorem, the acoustic waves with a specific wave vector ($\vec{k}$) in periodic structures can be expressed using Bloch states.[22] The Bloch states are wave functions with the

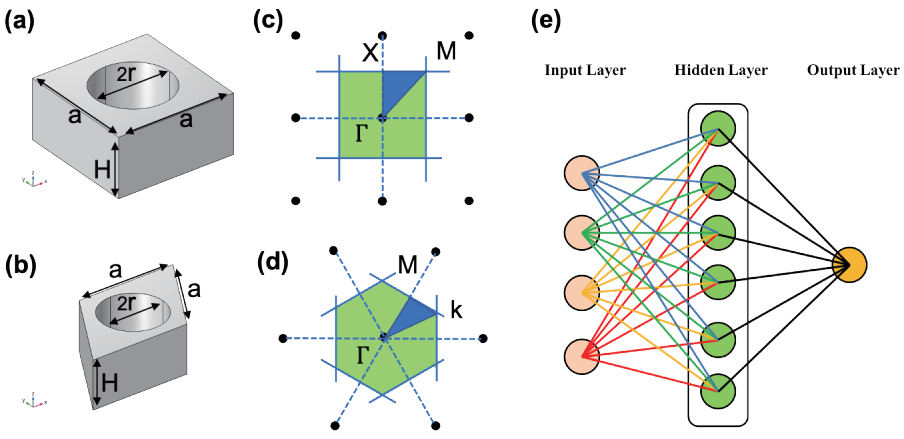

Fig. 1. (Color online) Schematic of unit cells of (a) square and (b) triangular lattice phononic crystal slabs. First Brillouin zones of (c) square and (d) triangular lattices. (e) Schematic of ANN.

same periodicities as the periodic structures. The Bloch states of certain $\vec{k}$ can be obtained by solving the eigen states and eigen frequencies of the unit cells with Floquet boundary conditions. We use the finite element method (FEM) to perform the eigen analysis. The FEM simulation is supported by a commercial software (COMSOL Multiphysics). The simulation domains in FEM are illustrated as Figs. 1(a) and 1(b). The software enables us to apply Floquet periodic boundary conditions at the boundaries vertical to *x*-*y* planes. The Floquet periodic boundary conditions are associated with the components of $\vec{k}$.

The green areas in Figs. 1(c) and 1(d) show the schematics of first Brillouin zones in the reciprocal space of the square and triangular lattices, respectively. All dispersion relations of acoustic waves in a phononic crystal can be represented by the relations between eigen frequencies and $\vec{k}$ within the Brillouin zones. The blue areas in Figs. 1(c) and 1(d) show the irreducible Brillouin zones, that is, the first Brillouin zones reduced by all of the symmetries. In most of the previous studies of phononic crystals, the band structures of phononic crystals represent the dispersion relations at the edges of irreducible Brillouin zones, i.e., the starting points of wave vectors are at Γ points and the end points of wave vectors sweep along the edges of irreducible zones, usually in the order of Γ-X-M-Γ for the square lattice and Γ-M-K-Γ for the triangular lattice. Therefore, a phononic band structure representing the dispersion relations composes of the wave vectors within the irreducible zone as the horizontal axis and the eigen frequencies of the eigen states at corresponding $\vec{k}$ vectors as the vertical axis. There are many orders of eigen states for each $\vec{k}$. We only extract five orders with the lowest eigen frequencies. This means that each $\vec{k}$ corresponds to five eigen frequencies.

The datasets for ANN training are obtained using FEM-calculated band structures with different geometrical parameters. On a single square lattice phononic crystal slab structure, the edge of the irreducible zone is divided into 75 points, i.e., there are 75 $\vec{k}$ vectors. There are 5 orders of eigen frequencies for each $\vec{k}$. Therefore, there are 375 (75 × 5) eigen frequencies for one single square lattice phononic crystal structure. We vary the r/a ratio from 0.15 to 0.45 in steps of 0.05. The H/a ratio is varied from 0.3 to 0.65 again in steps of 0.05. Thus, there are 56 square lattice phononic crystal structures and, consequently, a total of 21000 eigen frequencies in the datasets of the square lattice phononic crystal slab. In the datasets, the eigen frequency is the output target of the ANN. Each eigen frequency corresponds to a unique set of r/a ratio, H/a ratio, length of $\vec{k}$, and order number. This information is the input data for the ANN.

For the datasets of a triangular lattice of the phononic crystal slab, the edge of the irreducible Brillouin zone is divided into 151 points. The r/a ratio is varied from 0.15 to 0.4 in steps of 0.05. The H/a ratio is varied from 0.3 to 0.65 also in steps of 0.05. Therefore, there are 48 triangular lattice phononic crystal slab structures and a total of 36240 eigen frequencies in the datasets. Again, the eigen frequencies are the output targets of the ANN. The corresponding input data are r/a ratios, H/a ratios, lengths of $\vec{k}$, and order numbers.

A schematic of the ANN is illustrated in Fig. 1(e). We construct and train the ANNs using the function of fitting the regression in the deep learning toolbox of MATLAB. The values of the input data of r/a ratios, H/a ratios, lengths of $\vec{k}$, and order numbers are entered to the input layer. The corresponding eigen frequencies are used as output targets. We use two different hidden layer structures. The first one has one hidden layer with 100 neurons. The second one has two

hidden layers, with each layer having of 25 neurons. For the convenience of description, we refer to the first structure as NN1 and the second one as NN2. The ANNs are trained by the Levenberg–Marquardt backpropagation algorithm[23–24] using the datasets of band structures. The numbers of neurons in the hidden layers are optimized to achieve acceptable accuracies. Moreover, the training process does not require too much memory.

3. Results and Discussion

In this section, we discuss the ANN predictions for band structures of square and triangular lattice phononic crystal slabs individually. For both types of lattice, we investigate the prediction abilities and accuracies of NN1 and NN2 configurations.

The basic concept of backpropagation training of the ANN is reducing the inaccuracy between output targets and the predicted output by adjusting the connected weights in the neural network. In our case, the output targets are the eigen frequencies in the datasets. The predicted output is the output of the ANN computed from the input data, that is, r/a ratios, H/a ratios, lengths of wave vectors, and order numbers. The inaccuracy of the ANN is estimated using the mean square error of the target and predicted eigen frequencies. The datasets are divided into three groups: training group (70%), validation group (15%), and test group (15%). The data in the training group are used to adjust the connected weights in the neural network. The data in the validation group are used to validate the generalization of the network and to stop the training before overfitting. The data in the test group are not used in the training process and are preserved to test the performance of the network.

3.1 Square lattice phononic crystal slab

We trained the NN1 and NN2 configurations using the datasets of the square lattice phononic crystal slab. The trained NN1 and NN2 ANNs are respectively referred to as SNN1 and SNN2, and the training times are 194.5 s for SNN1 and 138.2 s for SNN2. We used SNN1 to predict the eigen frequencies of all input data in the datasets. The relationships between all predicted and target eigen frequencies are represented by the black circles in the dot chart in Fig. 2(a). The horizontal and vertical axes in Fig. 2(a) show the target and predicted eigen frequencies, respectively. If the prediction by SNN1 is 100% correct, all the dots should be located on the line of "Target frequency = Predicted frequency". Although there are some deviations between the positions of black circles and the line of "Target frequency = Output frequency" in Fig. 2(a), the distribution of black circles is mostly on the line of "Target frequency = Output frequency". We repeated the above-described process with SNN2. The dot charts of the target and predicted eigen frequencies of SNN2 are shown in Fig. 2(b). In Fig. 2(b), the distribution of black circles is also along the line of "Target frequency = Output frequency", although the deviations of black circles away from the line of "Target frequency = Output frequency" appear to be less than those in Fig. 2(a).

To compare the predicted accuracies of SNN1 with SNN2, we calculated the errors between the predicted and corresponding target eigen frequencies for all data and divided these errors

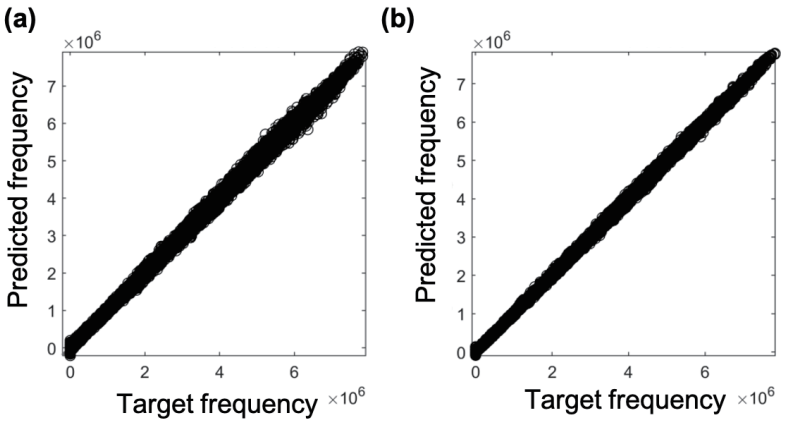

Fig. 2. Dot charts of relationships between all target and predicted frequencies of (a) SNN1 and (b) SNN2.

into 20 bins. Then, we plot the error histograms of SNN1 and SNN2 in Figs. 3(a) and 3(b), respectively. The horizontal axis represents the error range and the vertical axis represents the instances of predictions in each error range. The histograms indicate the errors of the training, validation, and test groups. The yellow lines in both histograms indicate the zero error positions. The errors are concentrated near the zero error for predictions by both SNN1 and SNN2. As seen in Fig. 3(a), for SSN1, the positive and negative maximum error ranges are centered at 0.499 and −0.45 MHz, respectively. Moreover, the positive and negative maximum error ranges of SNN2 are centered at 0.25 and −0.22 MHz, respectively. This shows that the accuracy of SNN2 is higher than that of SNN1, and the training time of SNN2 is also shorter than that of SNN1.

Figures 4(a) and 4(b) show the band structures of the square lattice phononic crystal slab. The r/a ratio is 0.3 and the H/a ratio is 0.5. The blue circles are the eigen frequencies calculated by FEM. The red dots in Figs. 4(a) and 4(b) are the eigen frequencies predicted by SNN1 and SNN2, respectively. Generally, the predicted results agree with the results of FEM. This means that SNN1 and SNN2 can well sketch the band structure. The significant differences between the plots in Figs. 4(a) and 4(b) are denoted by green circles marked A, B, and C. The prediction accuracy of SNN2 near the intersections of phononic bands is higher than that of SNN1. The intersections of phononic bands are important features of the phononic crystal. The phononic band gap, topological phononic cone, and negative refraction usually occur at frequencies near the intersections.

Figures 5(a) and 5(b) show the band structures of the square lattice phononic crystal slab whose r/a ratio is 0.12 and H/a ratio is 0.5. This r/a ratio is not included in the datasets. The blue circles are the eigen frequencies calculated by FEM. The red dots in Figs. 5(a) and 5(b) are the eigen frequencies predicted by SNN1 and SNN2, respectively. The predictions of SNN1 can roughly sketch the FEM results. However, the performance of SNN1 near the regions near the intersections of bands (marked A), the flat band (marked B), and the vertex of a band (marked C) is inaccurate. SNN2 performs better in these regions. Although the r/a ratio of 0.12 is not included in the datasets for training, the predictions of SNN2 still agree well with the results of FEM. This implies that the proposed ANN is generalized.

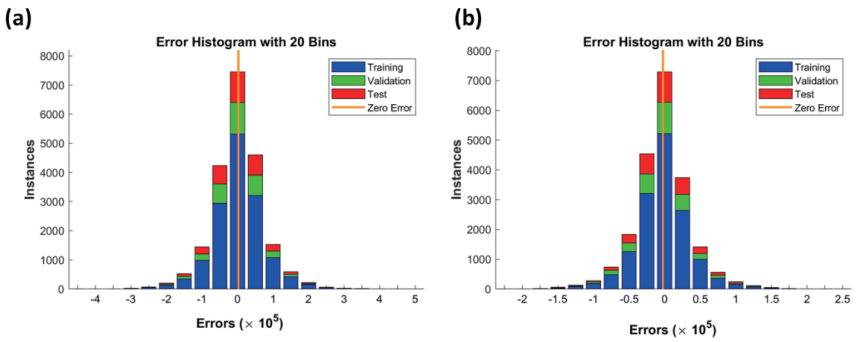

Fig. 3. (Color online) Error histograms of (a) SNN1 and (b) SNN2.

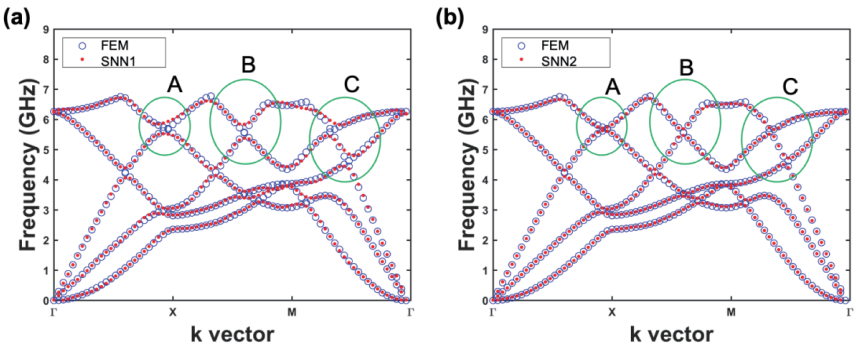

Fig. 4. (Color online) FEM-calculated band structure (blue circles) and band structures predicted by (a) SNN1 and (b) SNN2 (red dots). Structure: square lattice phononic crystal slab with r/a = 0.3 and H/a = 0.5.

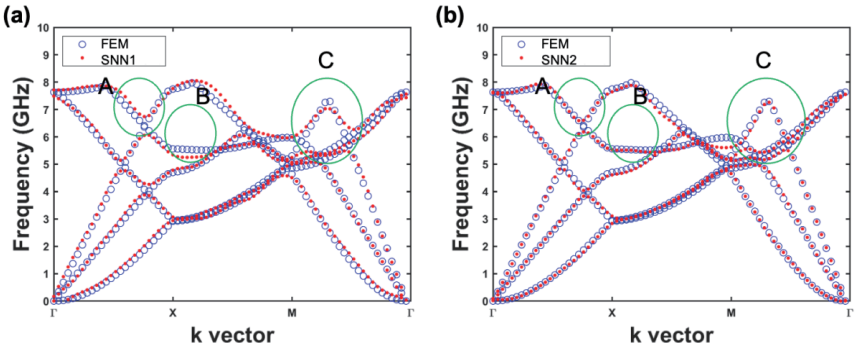

Fig. 5. (Color online) FEM-calculated band structure (blue circles) and band structures predicted by (a) SNN1 and (b) SNN2 (red dots). Structure: square lattice phononic crystal slab with r/a = 0.12 and H/a = 0.5.

3.2 Triangular lattice phononic crystal slab

In this section, we follow the same procedure as the ANN training of the square lattice to construct the ANNs for predicting the band structures of triangular lattice phononic crystal slabs. We again used NN1 and NN2 configurations in the training. The datasets used in the training process comprise the information of triangular lattice crystal slab band structures obtained by FEM. The trained NN1 and NN2 ANNs are referred to as TNN1 and TNN2, respectively. Because of the different simulation settings, the number of points in each band

structure is higher in the triangular lattice than in the square lattice, and therefore, the training times are 330.3 s for TNN1 and 370.5 s for TNN2, which are longer than in the case of the square lattice.

Figures 6(a) and 6(b) show the dot charts for the target and predicted frequencies of TNN1 and TNN2, respectively. The distributions of dots fall along the line "Target frequency = Predicted frequency". The deviations of the dots away from the line "Target frequency = Predicted frequency" are larger in Fig. 6(a) than in Fig. 6(b). This means that the predictions of TNN2 are more accurate than those of TNN1.

Figures 7(a) and 7(b) show the error histograms of the predicted eigen frequencies of TNN1 and TNN2, respectively. The errors between the target and predicted eigen frequencies are again divided into 20 bins. In Fig. 6(a), the positive and negative maximum bins are at 0.512 and −0.45 MHz, respectively. Moreover, in Fig. 6(b), the positive and negative maximum bins are at 0.211 and −0.22 MHz, respectively. This means that the predictions of TNN2 are more accurate than those of TNN1. However, the training time of TNN2 is longer than that of TNN1.

In Fig. 8, we show the triangular lattice phononic crystal slab band structures predicted by ANNs and those calculated by FEM. The predicted and calculated eigen frequencies are represented by red dots and blue circles, respectively. The r/a ratio of the phononic crystal slab is 0.3 and the H/a ratio is 0.5. The predicted eigen frequencies in Figs. 8(a) and 8(b) are obtained by

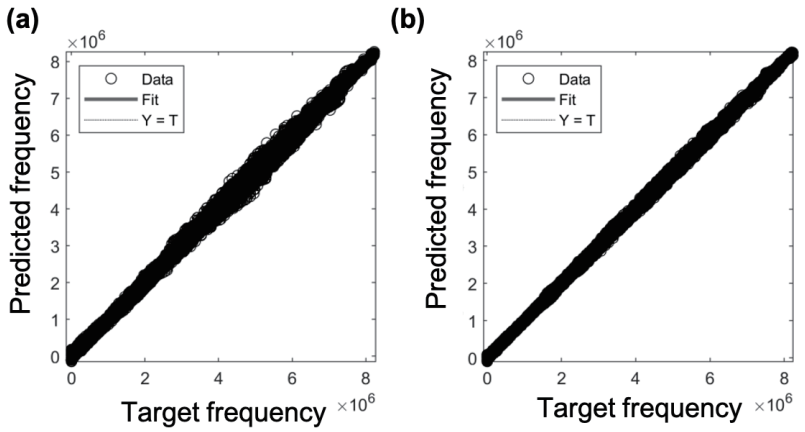

Fig. 6. Dot charts of relationships between target and predicted frequencies of (a) TNN1 and (b) TNN2.

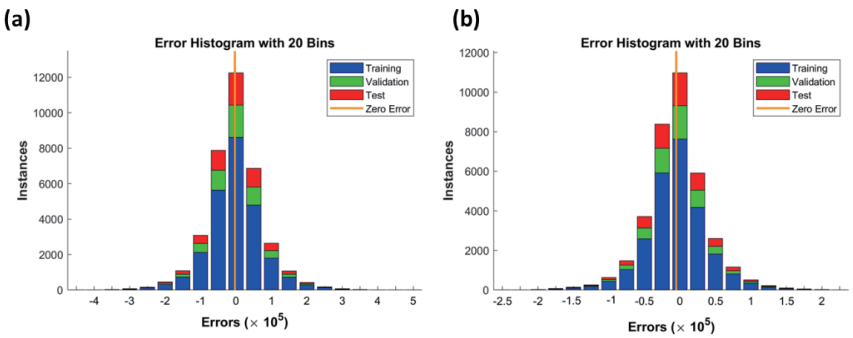

Fig. 7. (Color online) Error histograms of (a) TNN1 and (b) TNN2.

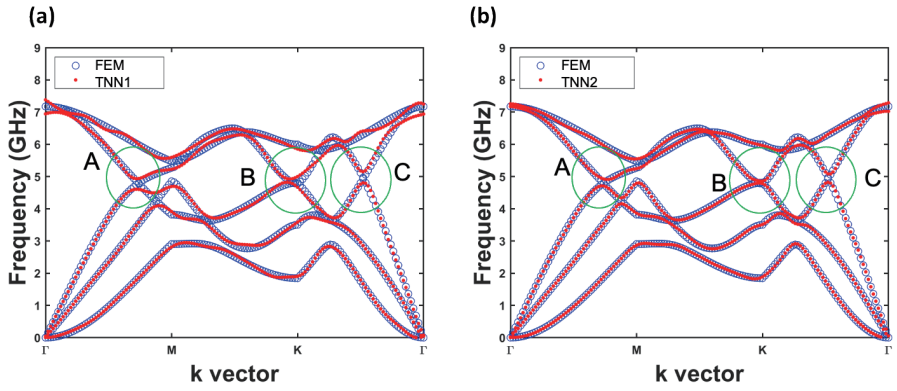

Fig. 8. (Color online) FEM-calculated band structure (blue circles) and band structures predicted by (a) TNN1 and (b) TNN2 (red dots). Structure: triangular lattice phononic crystal slab with r/a = 0.3 and H/a = 0.5.

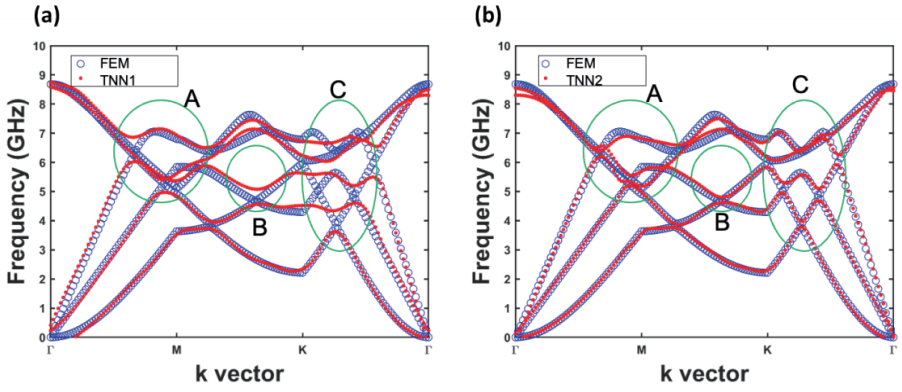

Fig. 9. (Color online) FEM-calculated band structure (blue circles) and band structures predicted by (a) TNN1 and (b) TNN2 (red dots). Structure: triangular lattice phononic crystal slab with r/a = 0.12 and H/a = 0.5.

TNN1 and TNN2, respectively. Comparing Fig. 8(a) with Fig. 8(b), we can see that the predicted results of TNN2 are smoother and more consistent than those of TNN1. Moreover, the prediction by TNN2 near the intersections (marked A, B, and C) is more accurate than that by TNN1.

We further use TNN1 and TNN2 to predict a triangular lattice phononic crystal slab that is not included in the training dataset. The r/a ratio is 0.12 and the H/a ratio is 0.5. The FEM-calculated band structures of this phononic crystal slab are denoted by blue circles in Figs. 9(a) and 9(b). The band structures predicted by TNN1 and TNN2 are represented by red dots in Figs. 9(a) and 9(b), respectively. In Fig. 9(a), the predictions by TNN1 only roughly agree with the results of FEM. The predicted results within the region marked C significantly deviate from the FEM calculation. The predictions by TNN2 in Fig. 9(b) are more accurate, especially in the regions marked A, B, and C. It can be concluded that TNN2 exhibits better generalization than TNN1.

4. Conclusions

We trained ANNs to predict the whole band structures of silicon phononic crystal slabs. The silicon phononic crystal slabs consisted of square and triangular lattice air cylinder arrays. We used FEM to calculate the band structures of various geometric parameters. The results of FEM calculation were used to train the ANNs. The input datasets consisted of r/a ratios, H/a ratios, lengths of wave vectors in the irreducible Brillouin zone, and order numbers of eigen states. The outputs corresponded to eigen frequencies. We investigated two configurations of ANNs: NN1 had only one hidden layer with 100 neurons and NN2 had two hidden layers, with each layer having 25 neurons. We compared the band structures calculated by FEM and predicted by trained ANNs. The NN2 configuration exhibited higher accuracies and better generalizations for both the square and the triangular lattices, especially in the details near the intersections of bands. The intersections of bands are frequently related to important features of phononic crystals, such as band gaps and topological phononics. The NN2 configuration has great potential for phononic crystal slab band structure predictions. The number of neurons in the hidden layers and the number of hidden layers were optimized to reduce the error. Although the number of neurons or hidden layers can be further increased, a significant accuracy improvement will not occur, but should the requirement for the memory of computers be raised, the training time might also be raised. In this study, although the training times of the NN1 and NN2 configurations did not show any specific relation of one being greater than the other, the training time is strongly related to the convergence of the neural network. The more complex the neural network configuration, the more difficult the convergence and the longer the training time required to achieve good accuracy. Our study revealed the potential of ANNs for phononic whole band structure prediction. The computation time of ANNs is one hundred times shorter than that of the FEM calculation. In contrast to previous studies that focused on certain features of the phononic crystal, the whole band structure may be more useful for the AI-assisted design of phononic crystals.

References

1 M. S. Kushwaha, L. D. P. Halevi, and B. Djafari-Rouhani: Phys. Rev. Lett. **71** (1993) 2022. https://doi.org/10.1103/PhysRevLett.71.2022
2 M. M. Sigalas and E. N. Economou: Solid State Commun. **86** (1993) 141. https://doi.org/10.1016/0038-1098(93)90888-T
3 Y.-L. Lee, M.-S. Chang, K.-H. Wei, T.-K. Li, C.-Y. Ni, C.-C. Chiu, Y.-P. Tsai, Y.-M. Weng, F.-L. Hsiao: AIP Adv. **9** (2019) 125102. https://doi.org/10.1063/1.5120547
4 Y. L. Lee, K. H. Wei, Y. P. Tsai, M. S. Chang, C. T. Chiang, W. S. Chang, C. C. Chiu, Y. Y. Wang, F. L. Hsiao: AIP Adv. **10** (2020) 085307. https://doi.org/10.1063/5.0020549
5 E. Yablonovitch: Phys. Rev. Lett. **58** (1987) 2059. https://doi.org/10.1103/PhysRevLett.58.2059
6 Z. Li, S. Yang, D. Wang, H. Shan, D. Chen, C. Fei, M. Xiao, and Y. Yang: Appl. Phys. Lett. **119** (2021) 073501. https://doi.org/10.1063/5.0058415
7 Z. Wang, F. Liu, S. Yu, S. Yan, M. Lu, Y. Jing, and Y. Chen: J. Appl. Phys. **125** (2019) 044502. https://doi.org/10.1063/1.5066034
8 P. Arrangoiz-Arriola, E. A. Wollack, M. Pechal, J. D. Witmer, J. T. Hill, and A. H. Safavi-Naeini: Phys. Rev. X **8** (2018) 031007. https://doi.org/10.1103/PhysRevX.8.031007
9 X. Liu, Q. Qiao, B. Dong, W. Liu, C. Xu, S. Xu, and G. Zhou: Int. J. Optomechatronics **15** (2021) 120. https://doi.org/10.1080/15599612.2021.1986612

10 A. I. Ovcharenko, C. Blanchard, J. Hugonin, and C. Sauvan: Phys. Rev. B **101** (2020) 155303. https://doi.org/10.1103/PhysRevB.101.155303
11 D. Qian: J Mater Sci **54** (2019) 4038. https://doi.org/10.1007/s10853-018-3124-4
12 T. Ma, Q. Fan, C. Zhang, and Y. Wang: J. Appl. Phys. **129** (2021) 145104. https://doi.org/10.1063/5.0040804
13 S. Teymouri, H. Ahmadi, and A. Rostami: Int. J. Mech. Sci. **207** (2021) 106658. https://doi.org/10.1016/j.ijmecsci.2021.106658
14 H. Huang, S. Huo, and J. Chen: Int. J. Mech. Sci. **198** (2021) 106391. https://doi.org/10.1016/j.ijmecsci.2021.106391
15 Z. Tian, C. Shen, J. Li, E. Reit, H. Bechman, J. E. S. Socolar, S. A. Cummer, and T. J. Huang: Nat. Commun. **11** (2020) 762. https://doi.org/10.1038/s41467-020-14553-0
16 C. Ho, E. Su, P. Li, M. J. Bolger, and H. Pan: Adv. Technol. Innov. **5** (2020) 76. https://doi.org/10.46604/aiti.2020.4278
17 Y. Yeo and K. Yen: Int. J. Eng. Technol. Innov. **11** (2021) 135. https://doi.org/10.46604/ijeti.2021.6891
18 Z. Li, H. Shen, Q. Chen, Y. Liu, S. You, and Z. He: ISPRS J. Photogramm. Remote Sens. **150** (2019) 197. https://doi.org/10.1016/j.isprsjprs.2019.02.017
19 S. An, C. Fowler, B. Zheng, M. Y. Shalaginov, H. Tang, H. Li, L. Zhou, J. Ding, A. M. Agarwal, C. Rivero-Baleine, K. A. Richardson, T. Gu, J. Hu, and H. Zhang: ACS Photonics **6** (2019) 3196. https://doi.org/10.1021/acsphotonics.9b00966
20 X. Li, S. Ning, Z. Liu, Z. Yan, C. Luo, and Z. Zhuang: Comput. Methods Appl. Mech. Eng. **361** (2020) 112737. https://doi.org/10.1016/j.cma.2019.112737
21 S. Han, Q. Han, and C. Li: Appl. Lett. Phys. **132** (2022) 154901. https://doi.org/10.1063/5.0111182
22 C. Kittel: Introduction to Solid State Physics (John Wiley & Sons, Inc, USA, 2004) Chap. 2.
23 H. Yu and B. M. Wilamowski: Intelligent Systems (Taylor & Francis Group, USA, 2011) Chap.12.
24 J. Rubio: IEEE Trans. Neural Networks Learn. Syst. **32** (2020) 3510. https://doi.org/10.1109/TNNLS.2020.3015200

About the Authors

Chi-Tsung Chiang received his M.S. degree from National Changhua University of Education (NCUE), Taiwan, in 2013. Currently, he is a Ph.D. candidate in the College of Photonics, National Changhua University of Education, Taiwan. He has been a researcher of metamaterials in NCUE since 2017. His current research interests include photonic crystals, phononic crystals, acousto-optic structures, and ultrasound structures.

Ying-Pin Tsai received his B.S. degree from the Department of Physics of National Changhua University of Education, Taiwan, in 2014 and his M.S. degree from the Graduate Institute of Photonics, National Changhua University of Education, Taiwan, in 2017. Currently, he is a Ph.D. candidate in the College of Photonics, National Yang Ming Chiao Tung University, Tainan City, Taiwan. He has been a researcher of metamaterials in National Yang Ming Chiao Tung University since 2018. His current research interests include photonic crystals, phononic crystals, acousto-optic structures, and ultrasound structures.

Wei-Shan Chang received her B.S. and M.S. degrees from Chung Shan Medical University, Taiwan, in 2008 and 2010, respectively. She is currently a Ph.D. student in the Institute of Photonics, National Changhua University of Education. Her research interests are in photonic and phononic crystals.

Fu-Li Hsiao received his B.S. degree from National Changhua University of Education, Taiwan, in 2002 and dual Ph.D. degrees from the National Central University, Taiwan, in 2008 and the University of Franche-Comté, France, in 2008. Since 2010, he has been a professor at the Institute of Photonics, National Changhua University of Education, Taiwan. His research interests are in photonic crystals, phononic crystals, optomechanics, and metamaterials.